Electrochimica Acta 210 (2016) 435–444

Contents lists available at ScienceDirect

Electrochimica Acta

journal homepage: www.elsevier.com/locate/electacta

Amine-appended polyaniline as a water dispersible electroactive polyelectrolyte and its integration into functional self-assembled multilayers

Waldemar A. Marmisollé[a,*], Eliana Maza[a,b], Sergio Moya[b], Omar Azzaroni[a]

[a] Instituto de Investigaciones Fisicoquímicas Teóricas y Aplicadas (INIFTA), Departamento de Química, Facultad de Ciencias Exactas, Universidad Nacional de La Plata (UNLP), CONICET 64 and 113, La Plata, Argentina[1]

[b] Soft Matter Nanotechnology Group, CIC biomaGUNE, Paseo Miramón 182, 20009 San Sebastián, Gipuzkoa, Spain

ARTICLE INFO

Article history:
Received 19 April 2016
Received in revised form 14 May 2016
Accepted 27 May 2016
Available online 27 May 2016

Keywords:
polyaminobenzylamine (PABA)
polyelectrolyte multilayers
layer-by-layer (LbL) assemblies
electroactive polymers
polyaniline (Pani)

ABSTRACT

We present an effective and simple method for the synthesis of poly(3-aminobenzylamine) (PABA) using a chemical oxidation strategy in aqueous solution. The polymer was characterized by NMR, LDI-TOF mass spectrometry, UV-visible, XPS and ATR-FTIR spectroscopies. Stable acidic dispersions were employed for the construction of layer-by-layer assembled films with polyanions, which effectively act as dopants of the electroactive component as revealed by spectroscopic analysis. The assembled films were electroactive in neutral solutions, probably owing to the combination of the doping effect by the polyanions and the self-doping effect of the protonated amino groups of the PABA backbone. These layers showed an electrocatalytic effect on the ascorbic acid oxidation. The advantages of employing PABA instead of polyaniline include improved electroactivity in neutral solution, good processability owing to its higher solubility in acidic solutions and increased interaction with anionic counterparts, which may propel its integration with electroactive biomolecules or conducting nanomaterials for the design of bioelectrochemical devices and energy storage applications.

1. Introduction

In the last decades, organic conducting polymers (CPs) have become interesting materials for many applications owing to their low cost, ease of synthesis and versatile electronic properties [1,2]. Within the vast universe of CPs, polyaniline (Pani) has been one of the most studied materials [3–5]. Its inexpensive simple synthesis, high conductivity and chemical stability have propelled its application in different areas from biosensing [6] to energy storage [7]. For biosensing applications, Pani-like materials offer the advantage of an adequate non-denaturing environment for the immobilization of redox enzymes and proteins and in some cases they can also act as physicochemical transducer of the chemical signals into an electrical response or simply mediate the electron transfer [6,8,9]. However, both mediation and transduction depend critically on the conducting and redox performances, which are generally excellent in acidic media but poor in neutral solutions. This is a clear disadvantage for most bioelectrochemical devices whose biochemical components are designed to operate efficiently at physiological pH. In some cases, the electroactivity of Pani in neutral solutions has been improved by incorporation of doping agents as polyanions [10–12] and complex anionic molecules [13] or conducting counterparts as metal nanoparticles [14] and carbon nanomaterials [15,16] yielding more complex materials or even composites. An alternative strategy to doping is the polymerization of substituted anilines, whose additional chemical groups can act as self-dopants of the resulting polyaniline in neutral pHs [17]. Particularly, in the case of polyaminobenzylamines, the protonable pendant amine groups confer additional charges to the polymer chains, which in turn improve the proton doping level and the electroactivity. Although low reactive, the backbone nitrogen groups of Pani have been used to link covalently the polymer through amide [18] and phosphoroamide [19] bonds in biodevices. The presence of additional more reactive primary amino groups would allow functionalization by addition of either chemical moieties or biorecognition elements yielding multifunctional materials [20].

In this sense, we have recently shown that it is possible to electrosynthesize copolymers of aniline and aminobenzylamines

* Corresponding author.
E-mail address: wmarmi@inifta.unlp.edu.ar (W.A. Marmisollé).
[1] http://softmatter.quimica.unlp.edu.ar.

http://dx.doi.org/10.1016/j.electacta.2016.05.182
0013-4686/

to produce amino-functionalized Pani-like films with enhanced electroactivity in neutral solution [21]. Although the electrochemical methods allow for a precise control of the amount of polymer, batch chemical synthesis would make possible a large-scale production of materials as it is necessary for some practical applications and for large production of devices. Chemical synthesis of Pani is simple and well-known, but its subsequent processability poses complex challenges [22]. Water dispersions of Pani are not stable over the long term. Most of the works on assemblies of Pani employ dispersions prepared based on the Rubner's method with small variations [23]. This procedure includes several laborious steps. Briefly, Pani is synthesized by oxidation with persulfate in acidic solution, then neutralized with NH_4OH, dried and redispersed in dimethylacetamide after several hours of stirring and sonication, and the remaining particles are filtered. This organic solution is then diluted with acidic water to form aqueous dispersions of pH about 2.5, which are said to be stable for some days. Significant effort has been devoted to improve the processability of Pani-like materials, by either post-synthesis chemical modification [24] or copolymerization [25,26].

On the other hand, the complementary properties of CPs and carbon nanomaterials, have recently promoted a great interest in producing composites for energy storage and sensing applications [7,27–29]. Although several methods have been developed for the construction of these complex interfaces [29], the layer-by-layer (LbL) assembly has become one of the most employed methods for coating a wide variety of substrates with films of well-ordered nanoarchitecture [30,31]. All LbL-based methods critically depend on the interaction between the counterparts, which is mainly electrostatic. The presence of additional protonable amino groups in the CPs could enhance this interaction improving the stability of the LbL assemblies.

Herein, we present a simple chemical method to obtain water dispersions of polyaminobenzylamines (PABA). The presence of additional amino groups in this Pani-like material yields good electroactivity in neutral solutions as desirable for the construction of functional bioelectrochemical assemblies. Furthermore, the protonable amino moieties allow both the preparation of stable aqueous dispersions and the integration of this material with negative counterparts for the construction of more complex electroactive LbL assemblies.

2. Experimental Section

2.1. Chemicals

Ammonium persulfate (APS), 3-mercapto-1-propanesulfonic acid sodium salt (MPS) and 3-aminobenzylamine (ABA) (Scheme 1) were purchased from Sigma-Aldrich. L-ascorbic acid (AA), HCl, KCl and sulfuric acid were purchased from Anedra. Poly(sodium 4-styrenesulfonate) (Mw 70 kDa) (PSS), poly(4-styrenesulfonic acid-co-maleic acid) sodium salt (Mw 20 kDa) (PSSMA) and polyethylenimine (Mw 10 kDa) (PEI) were also purchased from Sigma-Aldrich. All chemicals were employed as received without further purification. All solutions were prepared with Milli-Q water (18.2 MΩ cm).

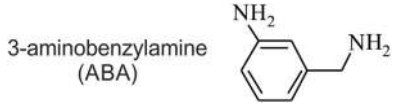

Scheme 1. Chemical structure of ABA.

2.2. PABA synthesis

The polymerization of PABA was achieved by chemical oxidation with APS. Briefly, a 50 mM ABA solution was prepared in water. The pH of this solution was about 9-10. This solution was magnetically stirred for 15 minutes. Then, solid APS was added to form a 50 mM solution under continuous stirring. Some minutes later, the initial transparent solution became dark brown and finally, dispersed brown solid particles were formed. After reaction, typically 1 hour, the pH of the solution was about 2.5. PABA was then purified by alkaline precipitation. Briefly, a 10% KOH solution was added to the synthesis solution to shift the pH to 10. Then, the solution was centrifuged at 7000 rpm for 10 minutes and the precipitate was re-dissolved in 0.5 M HCl up to the same initial volume. This solution was used as a stock solution for assembly (nominally about 5 mg mL^{-1}).

2.3. Instrumentation

Nuclear Magnetic Resonance (NMR) experiments were performed in D_2O using a 500 MHz Bruker AVANCE III NMR spectrometer equipped with a 1H/19 F BBI 5 mm probe. LDI-TOF mass analyses were performed on an Ultraflextreme III time-of-flight mass spectrometer equipped with a pulsed Nd:YAG laser (λ 355 nm) and controlled by FlexControl 3.3 software (Bruker Daltonics). The acquisitions were carried out in positive ion linear mode at a laser frequency of 1000 Hz. Laser power was adjusted for an optimal resolution and the spectra were obtained by addition of 1000 shots. Acquisition conditions were set as follows: Ion source 25 kV; ion source 2, 23.7 kV; lens voltage, 6.87 kV; detector gain 6.5x. LDI mass spectrum of PABA was performed from 0.5 M HCl solution.

Surface Plasmon Resonance (SPR) experiments were carried out by using a SPR Navi 210A instrument (BioNavis Ltd, Tampere, Finland). An electrochemistry flow cell (SPR321-EC, BioNavis Ltd.) was employed for all measurements. Gold sensors (BioNavis Ltd) were employed for SPR measurements were cleaned by immersion in boiling NH_4OH (28%)/H_2O_2 (100 vol) 1:1 for 15 min and then rinsed with water and ethanol. Injection was performed manually and SPR angular scans (785 nm laser) were recorded with no flow in the cell. Temperature was kept at 20 °C. All SPR experiments were processed using the BioNavis Data viewer software.

Atomic Force Microscopy (AFM) was performed with a Veeco Multimode AFM connected to a Nanoscope V controller was used to image the substrate. AFM measurements were performed in tapping mode in air using a TESP-V2 (Bruker, K = 42 N m^{-1}) cantilever.

X-ray Photoelectron Spectroscopy (XPS) was performed using a SPECS SAGE HR 100 system spectrometer. A Mg Kα (1253.6 eV) X-ray source was employed operating at 12.5 kV and 10 mA. Survey spectra were obtained with pass energy of 30 eV whereas 15 eV was employed for detailed spectra of C1s, N1s, and S2p regions. The take-off angle was 90° and operating pressure was 8 10^{-8} mbar. Quantitative analysis of spectra was carried out by using the Casa XPS 2.3. 16 PR 1.6 software, employing Shirley baselines and Gaussian\Lorentzian (30%) product functions. Surface-charging effects were corrected by setting the binding energy (BE) of the main component of the core level C1 s at 285 eV [32]. The full width at half maximum (fwhm), was kept fixed for different components of a given element. For quantitative N/S determinations, calculations were performed by recording the XPS spectrum of $(NH_4)_2S_2O_8$ powder in the same conditions as internal reference.

UV-visible absorption spectra were acquired with a Perkin-Elmer Lambda 35 UV–vis spectrometer. Fourier transform infrared spectroscopy in the attenuated total reflection mode (ATR-FTIR) was performed using a Varian 600 FTIR spectrometer equipped

with a ZnSe ATR crystal with a resolution of 4 cm^{-1}. Background-subtracted spectra were corrected for ATR acquisition by assuming a refractive index of 1.52 for all of the samples. Ellipsometry was performed with a spectroscopic ellipsometer (alpha-SE) from J. A. Woollam Co with three different incidence angles.

Dynamic light scattering (DLS) measurements were performed with a Zetasizer Nano (Nano ZSizer-ZEN3600, Malvern, U.K.) in water at 25 °C. The zeta-potential was determined from the electrophoretic mobility measured by Laser Doppler Velocimetry with a Zetasizer Nano. The Smoluchowski approximation of the Henry equation was employed for calculations. Measurements were performed in triplicate using disposable capillary cells (DTS 1061 1070, Malvern) at 25 °C with a drive cell voltage of 30 V and employing the monomodal analysis method.

Cyclic voltammetry (CV) was performed using a Gamry REF600 potentiostat in a conventional three electrodes electrochemical cell. The counter electrode was a Pt wire and a Ag/AgCl (3 M NaCl) electrode was employed as reference.

3. Results and Discussion

3.1. PABA Characterization

3.1.1. NMR

^{1}H NMR spectra acquired at different stages of the PABA synthesis are presented in Fig. 1. A 50 mM solution of ABA in D_2O was prepared (**spectrum a**). The NMR signals are in agreement with the 2 protons (3.62 ppm) from the methylene group and 4 aromatic protons of the disubstituted benzenic ring of ABA. After adding the oxidizing agent (50 mM APS, **spectrum b**) the methylene signal shifts to 4 ppm probably owing to the pH decrease caused by the APS. For comparison, the spectrum of an acidic ABA solution was added (ABA 50 mM, H_2SO_4 100 mM, **spectrum e**). In this case, the methylene signal is at 4.17 ppm and the aromatic signals also appeared at higher chemical shifts as a consequence of the protonation of both the aromatic and benzyl amino groups. After 40 min of reaction (**spectrum c**), the methylene signal appears at 4.16 ppm and the aromatic protons shows broader bands. The solution is dark and some aggregation occurs. After overnight incubation, the reaction solution was diluted 1:10 with 0.01 M H_2SO_4 in D_2O and sonicated. The ^{1}H-NMR results (**spectrum d**) show the aromatic protons between 7.25 and 7.5 ppm and the main signal attributed to methylene moiety at about 4.06. The ratio between aromatic to methylene H signals (right column in Fig. 1) indicates the polymerization has taken place as it changes from 2 for the monomer to ca. 1.5 for the polymer as it is was expected from the chemical structures in Fig. 1. The ^{13}C-NMR spectra of ABA and PABA, corresponding to ^{1}H-NMR spectra **(e)** and **(d)** in Fig. 1 respectively, are presented in the SI. As a consequence of polymerization, ^{13}C-NMR peaks become broader and appear at slightly lower chemical shifts. There is also a new peak at about 161 ppm that can be assigned to the C bound to N in a quinone-imine structure of the emeraldine-like state in PABA. This peak has been also reported for the chemical synthesis of Pani [33–35]. Finally, NMR data confirms that the methylene group remains next to a N moiety after the chemical polymerization. Further confirmation of the chemical structure was performed by mass spectrometry.

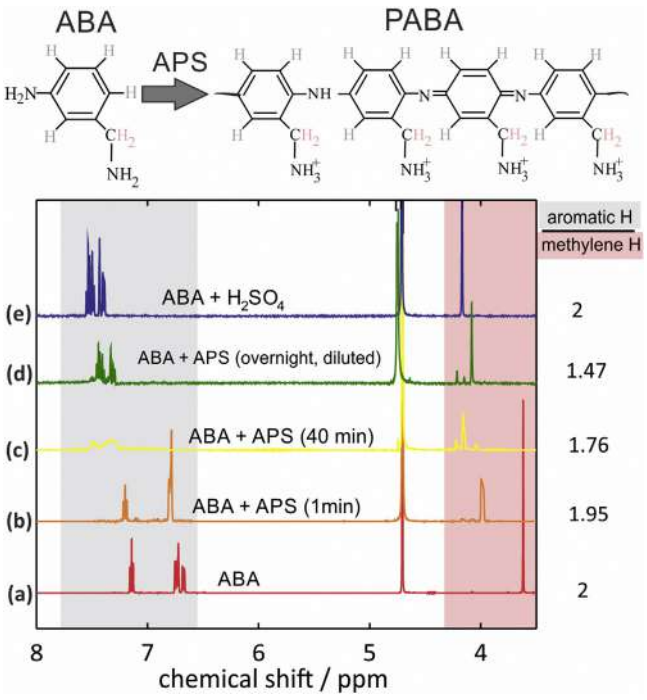

Fig. 1. ^{1}H-NMR spectra of different stages of the PABA synthesis in D_2O. Refer to main text for further details. On the top of the figure the chemical formula of ABA and the possible structures formed after polymerization in PABA. The methylene groups have been marked to emphasize that remain unaltered during polymerization.

3.1.2. Laser-Induced Desorption-Mass Spectrometry (LDI-MS)

MALDI-TOF has become a powerful tool for the structural analysis of synthetic polymers and macromolecules [36,37]. In the case of Pani, it has been found that the analysis by MALDI-TOF shows no molecular peaks, but only fragments. The use of matrix compounds does not generally help and it is preferable to employ directly laser desorption [38,39]. Additionally, Pani strongly absorbs radiation in the UV region, so laser-induced desorption (LDI) is possible [40]. Reported LDI-TOF results for Pani and poly (anisidine) show main peaks separated by 91 and 121 units, which agrees with the molecular weight of the monomer units and indicates that the peaks are owing to different number of monomers in the segments. There are also several secondary peaks separated by 15 units that corresponds to NH groups [38]. Successive peaks of $\Delta m/z = 14$-16 in Pani has been attributed to chain fragmentation under the desorption/ionization conditions [39,40]. With DHB as matrix, Pani oligomers up to 7 monomers were clearly observed, but poor signals were obtained for higher masses (up to 10 monomers) [39]. In other cases, oligomers up to 20 unit were detected by LDI-TOF [40]. The solvent-free LDI-TOF of Pani has been reported to be complex owing to the fragmentation of the phenyl groups induced by the laser. This fragmentation is inhibited when DHB is employed as matrix, absorbing most of the laser power and protecting the polymer chains from fragmentation [41]. Again, the presence of lateral peaks with $\Delta m/z = 15$ were observed and attributed to additional NH_2 or phenylene terminal groups present from the synthesis [42,43] or generated by the desorption/ionization conditions [40,42].

In the case of PABA, the LDI mass spectrum shows sets of peaks separated by about 120 units of mass (Fig. 2). The repetitive sets are notable up to about 1400 Da, which indicates oligomers of about 11-12 monomer units. These sets are composed by peaks separated by about 14–16 Da as it generally happens with Pani derivatives and indicates gain or loss of N, NH and NH_2 moieties [39,40].

3.1.3. Size and zeta-potential measurements

In order to study the incorporation of PABA into LbL assemblies with polyanions, the zeta-potential of acidic dispersions of PABA, poly(sodium 4-styrenesulfonate) (PSS) and poly(4-styrenesulfonic acid-co-maleic acid) sodium salt (PSSMA) were measured. Electrostatic interactions mostly dominate the LbL assembly of charged species. As it is an indication of the surface charge, zeta-

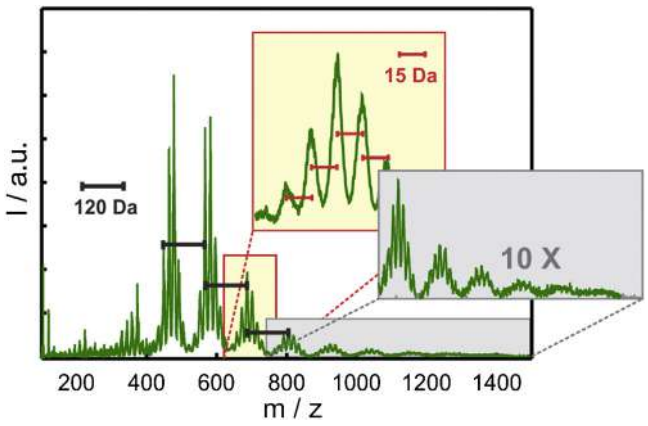

Fig. 2. LDI mass spectrum of PABA from 0.5 M HCl solution.

potential is a critical parameter in the study of polyelectrolytes as building blocks in interfacial nanoarchitectonics [44–46]. The electrolyte employed for DLS determinations and LbL assembly was 0.5 M HCl to guarantee the stability of the PABA dispersions. Solutions of concentration 1 mg mL^{-1} were prepared for the polyanions whereas PABA solution was obtained by dilution 1:100 from the stock solution with 0.5 M HCl (nominally 0.05 mg mL^{-1}). All solutions were filtered with a 0.22 μm filter (Schleicher & Schuell). No precipitation of PABA was observed even as long as several days after filtering. The zeta-potential values determined for PABA, PSS and PSSMA were 14 ± 2, -32 ± 5 and -20 ± 3 mV respectively. This is consistent with the protonation of PABA in acidic media and the negative charge in the polyanions is attributed to the sulfonic groups which remain dissociated even at pH about 0. The lower charge of PSSMA indicates that the MA residues are probably non-dissociated in these solutions (see ATR-FTIR results). Sizes determined by DLS (effective hydrodynamic diameters) were 10 ± 4 and 5 ± 3 nm for PSS and PSSMA respectively, based on the volume distribution fit (Fig. 3). This is consistent with the different molecular weight of the polyanions employed (70 and 20 kDa respectively). The z-average hydrodynamic diameter of PABA was determined to be 280 nm (PDI = 0.26), whereas the volume distribution fit was centered at 350 nm.

3.2. Layer-by-layer formation and structure of PABA-containing multilayers

The assembly of PABA and polyanions was monitored by SPR. Au sensors were first chemically modified with MPS to confer a net negative charge to the substrate. The functionalization was performed by immersion in 10 mM MPS aqueous solution overnight. Then the Au/MPS sensors were washed with water and ethanol and dried with N_2 flow. The assembly was performed by injecting the solutions in a 200 μL-volume quiescent SPR cell. Polyelectrolytes solutions (1 mL) were flowed through the cell and left 10 minutes to allow the adsorption, whereas the washing solutions (3 mL 0.5 M HCl) were left 5 min. Fig. 4 shows the evolution of the angle of minimum reflectivity of the Au sensors during the assembly of the LbL film of PABA with both PSS and PSSMA. As shown by this sensogram, the film effectively grows up and the deposited material remains after solvent washing. The changes of the minimum reflectivity angle are linear on the number of deposition cycles (Fig. 4), which indicates that the amount of material deposited is similar in the subsequent steps. After a deposition cycle, a bilayer (bl) is formed and the amount of deposited material is indicated by the number of bilayers (n). After eight deposition cycles, the sensors were washed with 0.5 M HCl and water and dried with N_2. The thickness of the assembled films was determined by spectroscopic ellipsometry (see SI), yielding 33 and 27 nm for films with PSS and PSSMA, respectively. The increment 3.3–4 nm/bl is similar to that reported for LbL assemblies of Pani with other polyelectrolytes [47,48] as well as with nanomaterials as carbon nanotubes [49] and graphene oxide [50,51]. This indicates that LbL deposition behavior is mainly determined by the Pani-like component. In the case of Pani fibers, the thickness reported per bilayer is lower than the fibers' diameter as determined by DLS, which indicates that the films are formed by patchy adsorption [52]. The same fact had been found in the assembly of Pani with polyelectrolytes, for which a minimum number of deposition cycles was required to obtain conductivity values similar to the bulk ones [47]. This reinforces the idea that several layers are needed to produce a fully continuous film with a percolation of the conducting components [29]. We have employed AFM to more deeply study the structure of the LbL assemblies. AFM images of 10-bilayer films are presented in Fig. 5. These images show the presence of globular aggregates of PABA. The root-mean-square surface roughness 5.7 nm and 5.3 nm for $(PABA/PSS)_{10}$ and $(PABA/PSSMA)_{10}$ assemblies respectively. In the case of Pani in LbL assemblies, the reported root-mean-squared roughness values depend on the quality of Pani dispersions. Values lower than 1 nm have been reported for LbL of Pani and polyanions from dispersions made by Rubner's method [48,23], but higher values (10–30 nm) have been also reported for the same systems assembled in other conditions [53]. In the case of assemblies of

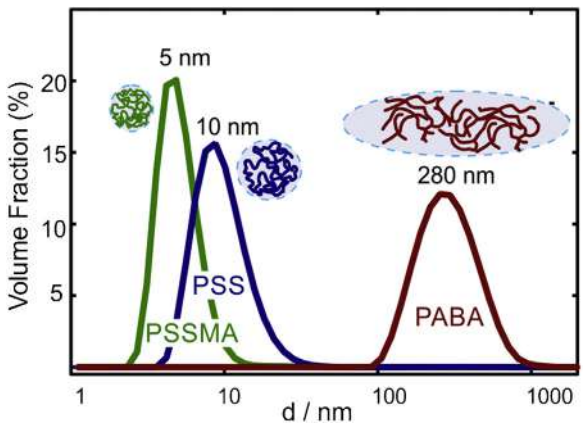

Fig. 3. Volume distribution determined by DLS for the polyelectrolytes in this work. Z-averaged diameters are indicated in the plot.

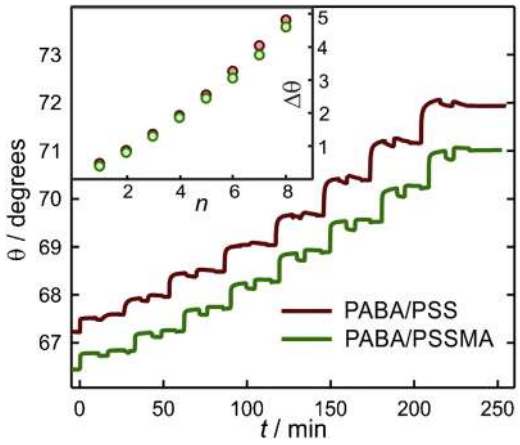

Fig. 4. Change in the minimum reflectivity angle of the SPR scan (measured at 785 nm) during the LbL formation of assemblies of PABA with PSS and PSSMA on Au/MPS substrates from 0.5 M HCl dispersions.

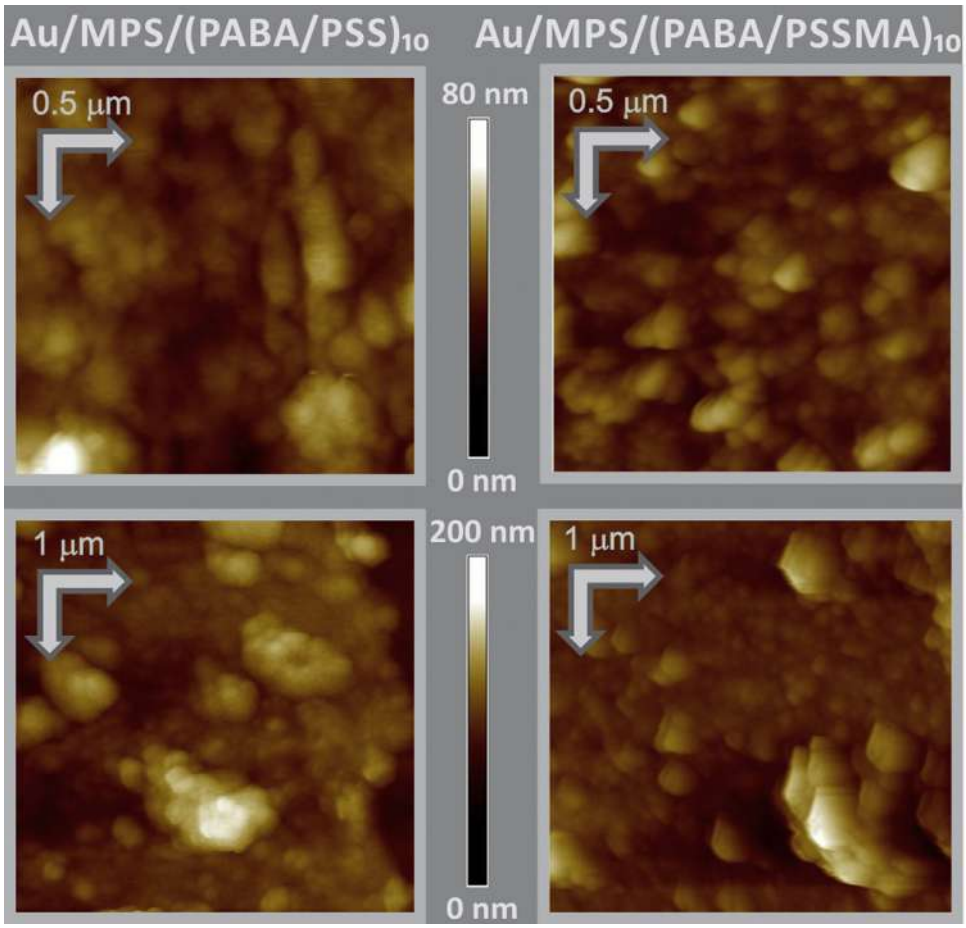

Fig. 5. AFM images of Au/MPS/(PABA/PSS)$_{10}$ (left) and Au/MPS/(PABA/PSSMA)$_{10}$ (right) assemblies.

Pani complexes or Pani with nanomaterials, reported values are even higher; i.e. 5–15 nm for Pani/graphene oxide [54,55,51], 20–40 nm for Pani/CNTs [56] and 60–600 nm for Pani complexes with polyelectrolytes [57]. In general, values higher than 1 nm indicate the deposition of Pani grains [54] or fibers yielding highly entangled porous films [56]. In some cases, however, the roughness has been reported to decrease by thermal treatment of the Pani/CNTs films [55,56] or reduction of the Pani/GO films [51], improving the mechanical stability.

The assemblies were also tested on glass substrates. For this purpose, glass slides were previously modified by PEI adsorption (1 mg mL^{-1}, 30 min incubation) to confer a positive surface charge to the substrate. The same solutions employed for the assembly on Au/MPS were used. Substrates were immersed in polyelectrolyte solutions for 12 minutes and then in the washing solution (0.5 M HCl) for 10 minutes. After LbL film deposition, the substrates were washed with 0.5 M HCl and water and dried with N_2 flow. The transmission UV-visible absorption spectra of the modified substrates with different number of bilayers up to 25 are also presented in Fig. 6. The absorption features correspond to that of the acidic PABA dispersion shown in Fig. 6(e). As in the case of Pani, the band bellow 350 nm is assigned to π-π^* transitions of the benzenic rings distorted by the presence of backbone amino groups [58–60]. The other band at about 500 nm could be

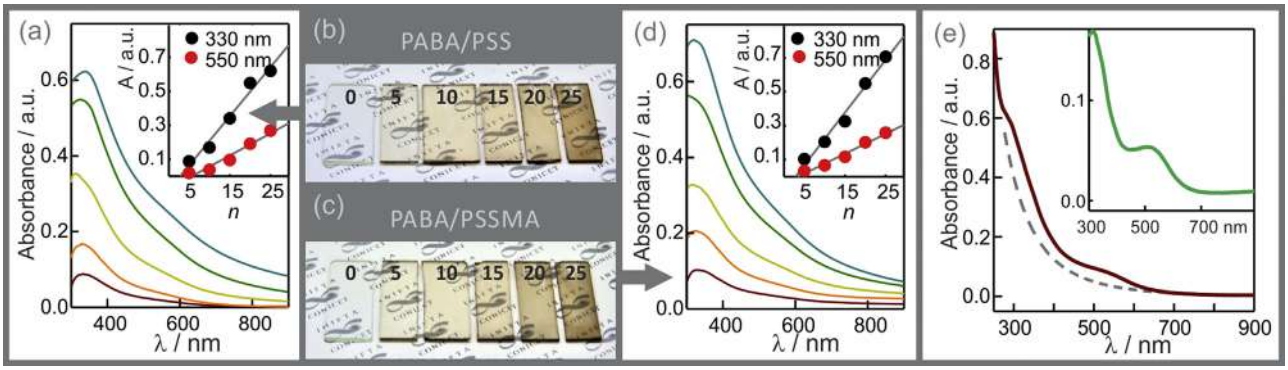

Fig. 6. UV-visible absorption spectra of LbL assemblies on glass substrates: (a) PABA/PSS, (d) PABA/PSSMA. The insets show the linear increase of the absorbance on the number of layers. (b-c) Digital images of the glass substrates after different number of deposition cycles. (e) UV-visible spectrum of PABA (ca. 0.25 mg mL^{-1}) in 0.5 M HCl. The inset shows the scattering corrected spectrum.

attributed to the excitonic transition that comes from an interchain absorption, leading to a separate charge state (molecular exciton) with a positive charge on a benzenic unit and a negative charge on a quinoid one [60–62]. Being this transition from the HOMO of benzenic to the LUMO of quinoid ring, it is sometimes indicated as (πB-πQ) [63]. As shown in the insets in Fig. 6(a) and (d), both absorption bands increase linearly with the number of deposition cycles, reinforcing the idea that a similar amount of polymer is deposited at each step.

The assemblies were further characterized by ATR-FTIR. The ATR-FTIR spectrum of PABA in the region 600 to 2000 cm^{-1} is shown in Fig. 7. The band at 1135 cm^{-1} has been assigned to the aromatic C-H in-plane bending in both IR [40,64] and Raman spectra of Pani and Pani assemblies [65]. Alternatively, it has been also assigned to a N = Q = N stretching mode [40,66]. This band is related to other band at 1612 cm^{-1}, assigned to the N = Q = N stretching [40,64,66,67]. There are also other less important bands at 1455 cm^{-1}, assigned to aromatic C-C [64] or C-N stretching [67]; and at 1500 cm^{-1}, which has been assigned to N-B-N stretching [66]; C-C in benzenic units [40,67]; N-H bending [40]; or Q = N-B stretching [67]. The vibrational spectroscopic information reveals that PABA presents a high degree of oxidized quinone-imine-like units. A complete FTIR characterization of PABA and a comprehensive list of the assignments of the bands are presented in the SI. The spectra of both the polyanions (commercial sodium salts) and the LbL assemblies are also presented in Fig. 7. The spectra of PSS in this region is dominated by the typical sulfonate bands: a doublet at about 1124 and 1178 cm^{-1} assigned to the asymmetric stretching of the sulfonate group [68] and a band at 1038 cm^{-1} assigned to a symmetric stretching of the same group [68,69]. There is also a band at about 1010 cm^{-1} that has been assigned to in-place aromatic CH bending [68,70]. Finally, the band at 830 cm^{-1} has been assigned to the out-of-plane aromatic CH deformation [69]. In the case of PSSMA there is also a band at about 1580 cm^{-1} attributed to the asymmetric stretching of the dissociated carboxylate group [71] and a lower band at 1410 cm^{-1} assigned to the symmetric stretching [71,72]. In the case of the assemblies, the FTIR confirms the presence of the chemical moieties of both components. The position of the sulfonate bands is basically the same, which shows that they remain in the salt form. Contrarily, in the case of PABA/PSSMA, there is also a shoulder at about 1710 cm^{-1} (arrow in Fig. 7) that can be assigned to the protonated carboxylic moiety as a consequence of the protonation of the maleic units in the assembling conditions.

To gain additional information on the composition and chemical state, we have performed XPS of the LbL assembled films. The N1 s region of XPS spectra of PABA and its assemblies with polyanions are depicted in Fig. 8. Based on works on Pani, we have already assigned the N1 s contributions in a previous work for the case of electrosynthesized PABA [21]. The N1 s core spectrum level of PABA can be deconvoluted into 5 peaks (fwhm 1.5 eV) (Table 1). The backbone N atoms can be considered to contribute with 4 bands corresponding to the uncharged N species (neutral imine [32,73–75] and neutral amine [73,75]) and positive N species from oxidized secondary amines (delocalized polaron-type structure) [73–76] and protonated imine (localized bipolaron-type structure) [73,75]. In the case of the primary amine pending moieties, the contributions are expected to appear at about 399 eV (indistinguishable from the backbone neutral amines) and 401 eV for the neutral and protonated forms respectively [77,78]. Results of fitting with these five components are shown in Fig. 8 and Table 1. The proportion of oxidized forms of N (polaron and imine structures, BE > 400 eV) increases when interacting with the polyanions, which reveals the role of the polyanions as dopants in the assembly. This is a proof of the chemical interaction between both components within the composite material which promotes an increased doping-state. This doping effect has been shown to be the responsible for the increased electrochemical performance of Pani composites in neutral solutions [79–81]. C1s and S2p XPS regions are presented in the SI. There are no major differences between PSS and PSSMA with the exception of the presence of a COO component signal in the case of the copolymer owing to the maleic units. Interestingly, there is some signal of S also in the case of chemically synthesized PABA. This could be attributed to some residual sulfate anions from the synthesis that could be retained within the PABA fibers as dopants. Moreover, the sulfur-to-nitrogen (S/N) ratio is lower in the case of the copolymer probably

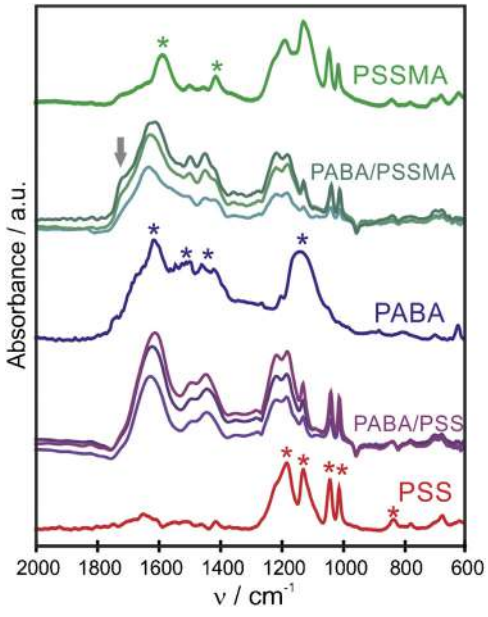

Fig. 7. ATR-FTIR spectra of components and assemblies deposited on Au substrates. From bottom to top: PSS, PABA/PSS assemblies with 10, 14 and 18 bilayers, PABA, PABA/PSSMA assemblies with 10, 14 and 18 bilayers, and PSSMA. Stars indicate bands assigned in the main text.

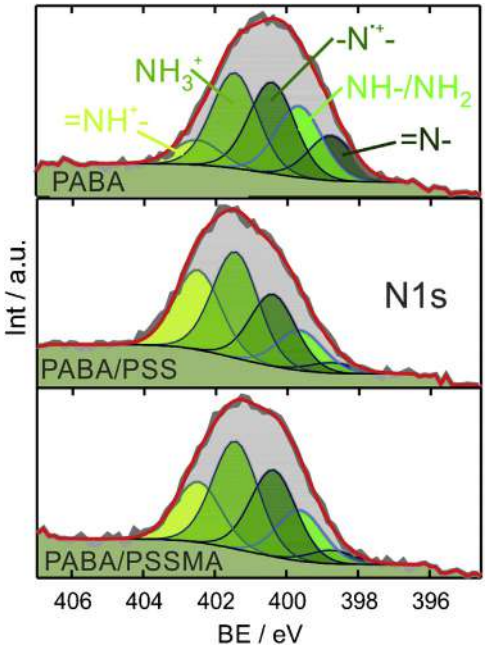

Fig. 8. N1 s XPS spectra of PABA and PABA/polyanion assemblies (10 bl). Grey lines are experimental spectra; red lines mean the global fittings.

Table 1
N1 s core XPS components of PABA and LbL assemblies (fwhm = 1.5 eV) and atomic compositions fitted.

Component	=N—	—NH—/NH_2	—$N^{\cdot+}$—	—NH_3^+	=NH^+—	S/N
BE (eV)	398.8	399.7	400.4	401.5	402.5	
PABA	14%	22%	28%	29%	7%	0.09
PABA/PSS	3%	13%	23%	35%	26%	0.64
PABA/PSSMA	4%	16%	27%	34%	19%	0.43

owing to the lower proportion of sulfonic groups. The interaction with the polyanions induces a higher proportion of the charged forms of the PABA units. This proportion is higher in the case of PSS, which is consistent with the idea that the maleic units of PSSMA are not dissociated in the acidic assembling conditions as also inferred from the FTIR results. However, as indicated by the SPR and UV-visible results, this does not affect the film formation, which is essentially the same as with PSS. This is not surprising as Pani has been also reported to form LbL assemblies with nonionic polymers via hydrogen bonding formation [48], as not all backbone N atoms are expected to be protonated even in acidic solutions [82].

3.3. Electrochemical Response of PABA and the LbL Assemblies

The electroactivity of the LbL assembled films was studied by cyclic voltammetry. Firstly, the voltammetric response of the chemically synthesized PABA block was evaluated in acidic solution (Fig. 9(a)). For this purpose, PABA was previously adsorbed on a MPS-modified gold electrode by immersion in the stock solution for 10 min. The linear dependence of the peak current on the sweep rate (Fig. 9(b)) confirms that it corresponds to the electron-transfer process of an adsorbed redox couple [83]. As it happens with the electrosynthesized PABA, there is not only a single redox couple but several peaks corresponding to different redox transformations [21]. The voltammetric response of an LbL assembly of PABA and PSS in the same solution is presented in Fig. 9(c). As shown in this figure, there is an increase in the voltammetric current as the number of deposition cycles increases (arrows), showing that it is possible to build an electroactive LbL assembly of PABA. At this high sweep rate, there is no defined redox peaks but a pseudocapacitive-like response. Furthermore, the voltammetric charge reaches a *plateau* on the number of deposited layers, which indicates that the charge transfer mechanism is effective up to about 8 bilayers (Fig. 9(d)). This indicates that the presence of the non-electroactive polyelectrolyte leads the formation of linearly increasing LbL assemblies, but it somehow limits the dynamics of the charge transport across the assemblies. Similar results were obtained for the PABA/PSSMA assemblies.

The electro-oxidation of ascorbic acid (AA) onto these modified electrodes was also studied by CV (Fig. 10). The biochemical importance of AA has promoted an intense work in the field of electrochemical sensing and several aspects of the electrochemistry of AA are well-known [84]. Even, it has been extensively employed to evaluate the electroactivity of Pani-based modified electrodes in neutral solutions [79,80,85]. Here, AA will be employed as a probe for testing the ability of the chemically synthesized PABA assemblies to interact with biologically relevant species and mediate electron transfer in neutral solution. As compared with the Au/MPS control substrate, the LbL-modified electrodes show an increase in the oxidation current with a lowering of the onset potential (Fig. 10). These results not only indicate that the assemblies are electroactive but also show the existence of an electrocatalytic effect [86]. Similar results are presented in the **SI** for PABA/PSSMA assemblies. The linear increase of the peak current on the AA concentration suggests that this system could be employed for voltammetric sensing. Typically, for thicker films the outer parts of the assemblies are not electrochemically connected and they block the interaction with the electroactive species in solution. This is a usual situation found in the electrochemical performance of LbL assemblies based on Pani. However, a strategy employed to improve the electrical connectivity in Pani assemblies has been the usage of conducting carbon nanomaterials. Being Pani not conducting at neutral pH, these building blocks could provide the necessary electronic connection within the films. In a recent work, chemically polymerized Pani assembled PSS-grafted graphene sheets was tested as an amperometric sensor of H_2O_2 in neutral solution [87]. With the increasing number of bilayers, the electroactive area of the electrode becomes larger, which can effectively improve the electrochemical response. However, further increase led to a decrease in the peak current, which was attributed to the blocking of the electron transfer from the substrate to the electrode by the non-conducting polymer, with an optimum number of 6 bilayers. For the first bilayers in an LbL assembly there is always a significant degree of interdigitation between layers as for these layers usually the surface coverage is not complete. At a certain number of layers

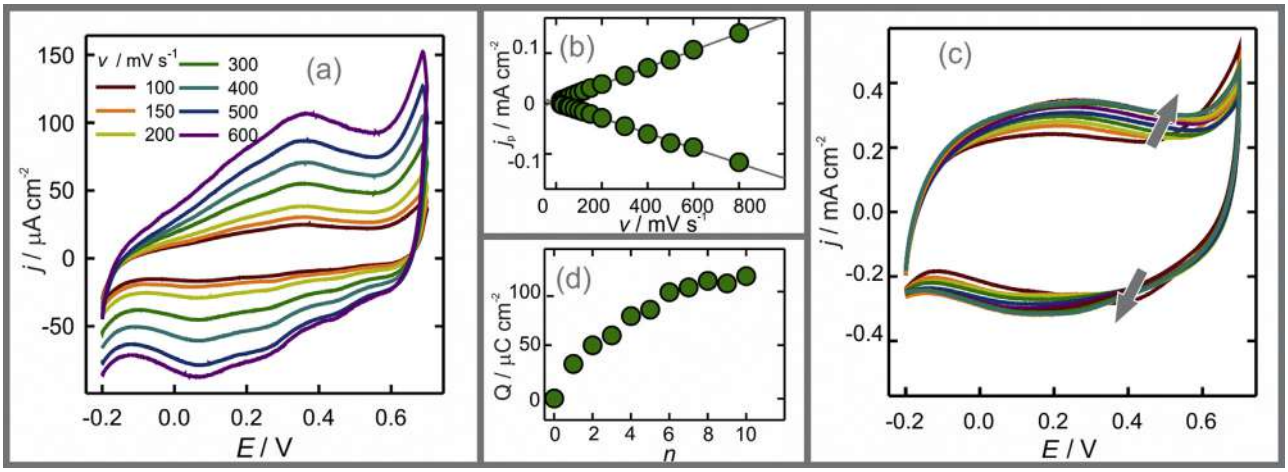

Fig. 9. (a) CV response of a Au/MPS/PABA electrode at different sweep rates in 0.5 M HCl and (b) sweep rate dependence of the current for the anodic (0.36 V) and cathodic (0.065 V) main peaks. (c) CV response of an Au/MPS/(PABA/PSS)$_n$ electrode for increasing number of bilayers (n) from 0 to 10 at 0.5 Vs^{-1} in 0.5 M HCl and (d) voltammetric integrated charge as a function of n.

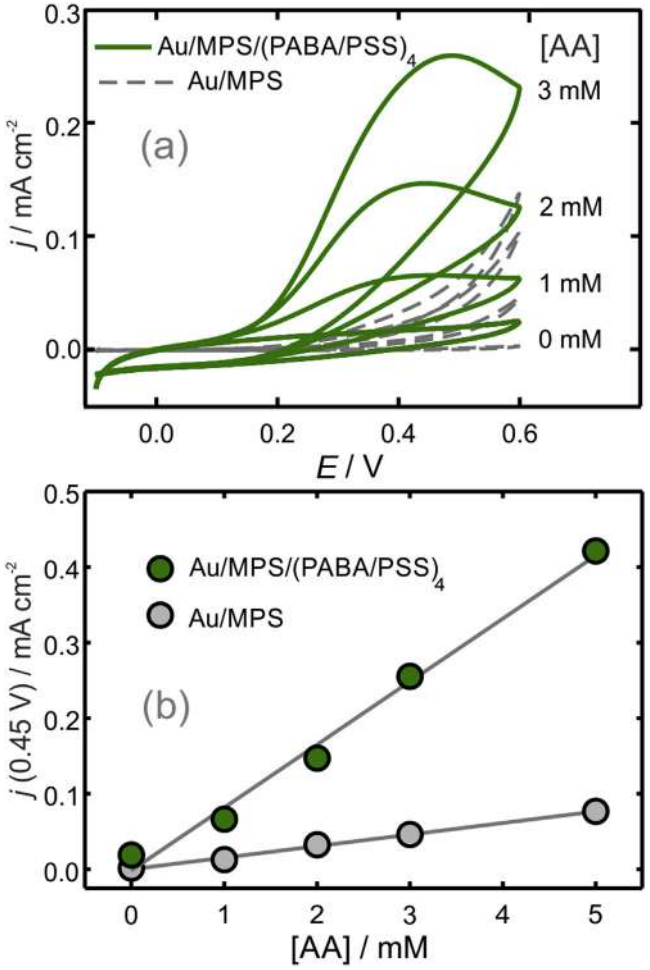

Fig. 10. (a) Ascorbic acid electro-oxidation on Au/MPS (dash line) and an LbL-modified electrode Au/MPS/$(PABA/PSS)_4$ (solid line) at 0.01 V s^{-1} in 0.1 M KCl 10 mM HEPES buffer pH 7. (b) Current density at 0.45 V as a function of the AA concentration for these electrodes.

the coating will be denser and interdigitation will decrease, reducing for our case with PABA the electronic connectivity. Even in LbL assemblies of reduced graphene oxide chemically modified by a cationic ionic liquid and sulfonated Pani [88], the voltammetric response in the presence of H_2O_2 in neutral PBS showed an increased cathodic current after the polymer reduction peak with an optimum amperometric performance for 8 bl. A similar situation was reported for the LbL assembly of Pani and oxidized MWNTs, which shows a better response towards H_2O_2 for 5 bilayers and this number was selected for the construction of a choline biosensor [89]. In other case, LbL films of Pani and PSS-capped MWNTs were reported to be electroactive in neutral PBS solution with a quasi-reversible unique couple and was shown to amperometrically sense H_2O_2 [90]. In this case, the electrochemically active material increased up to 7 bilayers, but a limiting value was obtained after further deposition cycles.

To study the influence of the electrochemical connectivity in PABA/polyanions assemblies, two thicknesses were compared: about 15 nm (4 bl, below the connectivity limit determined in acidic solution) and 50 nm (14 bl, within the plateau reached in Fig. 9(d)). Results are presented in the SI. Previous results on electrochemically synthesized films showed that at low sweep rate, the global process is AA diffusion-limited [21]. The AA must diffuse through the outer polyelectrolyte layers before reacting on the electroactive part of the assembly, being this process slower for thicker films. In the case of the LbL assemblies of PABA/polyanions, this yields a decrease of the AA oxidation current. The decrease of AA voltammetric current is lower in the case of the PSSMA (17% for PSSMA and 35% for PSS, see SI) and it could be related to the additional charges that can be induced in the maleic units when changing from the acidic assembling conditions to the neutral pH as it was recently reported for non-electroactive polyelectrolyte multilayers [91]. The additional charges could be responsible for a higher doping and the better electrochemical connection in neutral solution. From comparison with previous published results mentioned above on the electrochemical performance of the LbL assemblies of Pani and carbon nanomaterials, it can be seen that the PABA assemblies studied in this work show similar results even when the simple polyelectrolytes employed as counterparts are neither conducting nor electroactive. This could be attributed to the increased electroactivity of PABA as compared with Pani in neutral solution [21]. These promissory results open the door to the assembly of PABA with carbon nanomaterials to further increase the electrochemical connectivity.

4. Conclusions

In summary, we have presented a method to obtain water dispersions of polyaminobenzylamine by chemical oxidation of ABA. The procedure is simple and does not involve laborious steps, yielding dispersions that remain stable in acidic solution. The resulting polymer was characterized by diverse techniques and dispersions were employed for the construction of LbL assemblies with polyanions. The assemblies presented a linear dependence on the number of deposition cycles up to 25 bl and the spectroscopic characterization showed a doping effect of the anionic counterpart that indicates an integration of the diverse counterparts within the films. Additionally, the assemblies were electroactive both in acidic and neutral solutions. The good electroactivity at pH 7 is probably owing to the combination of the doping effect by the polyanions and the self-doping effect of the protonated amino groups of the PABA backbone. Even, the PABA/polyanions LbL-modified electrodes showed electrocatalysis of the ascorbic acid oxidation in neutral solutions. As the number of bilayers increases, the electrochemical response decreases probably due to the lower interdigitation of the successive layers and the blocking effect of the non-conducting polyanions.

The present results also open the door to further studies involving the assembly of PABA with other electroactive biomolecules for the construction of bioelectrochemical devices or even other conducting counterparts, e.g.: carbon nanomaterials, for the construction of highly interconnected electroactive films for energy storage applications.

Acknowledgement

The authors acknowledge financial support from ANPCyT (PICT 2010-2554, PICT-2013-0905), Universidad Nacional de La Plata (PPID-X009), Consejo Nacional de Investigaciones Científicas y Técnicas (CONICET) (PIP 11220130100370CO), Marie Curie project "Hierarchical functionalization and assembly of Graphene for multiple device fabrication" (HiGRAPHEN) (Grant ref: 612704), Fundación Petruzza and the Austrian Institute of Technology GmbH (AIT–CONICET Partner Lab: "Exploratory Research for Advanced Technologies in Supramolecular Materials Science"—Exp. 4947/11, Res. No. 3911). Technical NMR support by Dr. Marco Marradi and helpful assistance with digital images by Dr. M. L. Cortez are gratefully acknowledged. W.A.M. and O.A. are CONICET

fellows. SM acknowledges the project MAT2013-48169-R from the Spanish Ministry of Economy (MINECO).

Appendix A. Supplementary data

Supplementary data associated with this article (Ellipsometric, spectroscopic and electrochemical results on PABA and LbL assemblies) can be found, in the online version, at http://dx.doi.org/10.1016/j.electacta.2016.05.182.

References

[1] G. Inzelt, Conducting Polymers: A New Era in Electrochemsitry, 2nd ed, Springer-Verlag, Berlin Heidelberg, 2012.
[2] J. Heinze, B.A. Frontana-Uribe, S. Ludwigs, Electrochemistry of conducting polymers-persistent models and new concepts, Chem. Rev. 110 (2010) 4724–4771.
[3] S. Bhadra, D. Khastgir, N.K. Singha, J.H. Lee, Progress in preparation, processing and applications of polyaniline, Prog. Polym. Sci. 34 (2009) 783–810.
[4] G. Ćirić-Marjanović, Recent advances in polyaniline research: Polymerization mechanisms, structural aspects, properties and applications, Synth. Met. 177 (2013) 1–47.
[5] J. Stejskal, M. Trchová, P. Bober, P. Humpolíček, V. Kašpárková, I. Sapurina, et al., Conducting Polymers: Polyaniline, Encycl. Polym. Sci. Technol., John Wiley & Sons Inc., 2015.
[6] C. Dhand, M. Das, M. Datta, B.D. Malhotra, Recent advances in polyaniline based biosensors, Biosens. Bioelectron. 26 (2011) 2811–2821.
[7] N.A. Kumar, J.-B. Baek, Electrochemical supercapacitors from conducting polyaniline-graphene platforms, Chem. Commun. 50 (2014) 6298–6308.
[8] N.J. Ronkainen, H.B. Halsall, W.R. Heineman, Electrochemical biosensors, Chem. Soc. Rev. 39 (2010) 1747–1763.
[9] R.M. Iost, F.N. Crespilho, Layer-by-layer self-assembly and electrochemistry: applications in biosensing and bioelectronics, Biosens. Bioelectron. 31 (2012) 1–10.
[10] M.-K. Park, K. Onishi, J. Locklin, F. Caruso, R.C. Advincula, Self-Assembly and Characterization of Polyaniline and Sulfonated Polystyrene Multilayer-Coated Colloidal Particles and Hollow Shells, Langmuir. 19 (2003) 8550–8554.
[11] S. Tian, A. Baba, J. Liu, Z. Wang, W. Knoll, M.-K. Park, et al., Electroactivity of Polyaniline Multilayer Films in Neutral Solution and Their Electrocatalyzed Oxidation of β-Nicotinamide Adenine Dinucleotide, Adv. Funct. Mater. 13 (2003) 473–479.
[12] O.A. Raitman, E. Katz, A.F. Bückmann, I. Willner, Integration of Polyaniline/Poly (acrylic acid) Films and Redox Enzymes on Electrode Supports: An in Situ Electrochemical/Surface Plasmon Resonance Study of the Bioelectrocatalyzed Oxidation of Glucose or Lactate in the Integrated Bioelectrocatalytic System, J. Am. Chem. Soc. 124 (2002) 6487–6496.
[13] Q. Zhang, A. Prabhu, A. San, J.F. Al-Sharab, K. Levon, A polyaniline based ultrasensitive potentiometric immunosensor for cardiac troponin complex detection, Biosens. Bioelectron. 72 (2015) 100–106.
[14] E. Granot, E. Katz, B. Basnar, I. Willner, Enhanced Bioelectrocatalysis Using Au-Nanoparticle/Polyaniline Hybrid Systems in Thin Films and Microstructured Rods Assembled on Electrodes, Chem. Mater. 17 (2005) 4600–4609.
[15] X. Feng, H. Cheng, Y. Pan, H. Zheng, Development of glucose biosensors based on nanostructured graphene-conducting polyaniline composite, Biosens. Bioelectron. 70 (2015) 411–417.
[16] E. Granot, B. Basnar, Z. Cheglakov, E. Katz, I. Willner, Enhanced Bioelectrocatalysis Using Single-Walled Carbon Nanotubes (SWCNTs)/Polyaniline Hybrid Systems in Thin-Film and Microrod Structures Associated with Electrodes, Electroanalysis 18 (2006) 26–34.
[17] B.A. Deore, I. Yu, M.S. Freund, A switchable self-doped polyaniline: interconversion between self-doped and non-self-doped forms, J. Am. Chem. Soc. 126 (2004) 52–53.
[18] S.K. Arya, A. Dey, S. Bhansali, Polyaniline protected gold nanoparticles based mediator and label free electrochemical cortisol biosensor, Biosens. Bioelectron. 28 (2011) 166–173.
[19] Y. Bo, H. Yang, Y. Hu, T. Yao, S. Huang, A novel electrochemical DNA biosensor based on graphene and polyaniline nanowires, Electrochim. Acta 56 (2011) 2676–2681.
[20] W.A. Marmisollé, J. Irigoyen, D. Gregurec, S. Moya, O. Azzaroni, Supramolecular Surface Chemistry: Substrate-Independent Phosphate-Driven Growth of Polyamine-Based Multifunctional Thin Films, Adv. Funct. Mater. 25 (2015) 4144–4152.
[21] W.A. Marmisollé, D. Gregurec, S. Moya, O. Azzaroni, Polyanilines with Pendant Amino Groups as Electrochemically Active Copolymers at Neutral pH, ChemElectroChem 2 (2015) 2011–2019.
[22] J. Ruiz, B. Gonzalo, J.R. Dios, J.M. Laza, J.L. Vilas, L.M. León, Improving the Processability of Conductive Polymers: The Case of Polyaniline, Adv. Polym. Technol. 32 (2013) E180–E188.
[23] A.C. Fou, M.F. Rubner, Molecular-Level Processing of Conjugated Polymers. 2. Layer-by-Layer Manipulation of In-Situ Polymerized p-Type Doped Conducting Polymers, Macromolecules 28 (1995) 7115–7120.
[24] M. Jaymand, Recent progress in chemical modification of polyaniline, Prog. Polym. Sci. 38 (2013) 1287–1306.
[25] M.T. Nguyen, P. Kasai, J.L. Miller, A.F. Diaz, Synthesis and Properties of Novel Water-Soluble Conducting Polyaniline Copolymers, Macromolecules 27 (1994) 3625–3631.
[26] M.T. Nguyen, A.F. Diaz, Water-Soluble Poly(aniline-co-o-anthranilic acid) Copolymers, Macromolecules 28 (1995) 3411–3415.
[27] Q. Wu, Y. Xu, Z. Yao, A. Liu, G. Shi, Supercapacitors Based on Flexible Graphene/Polyaniline Nanofiber Composite Films, ACS Nano 4 (2010) 1963–1970.
[28] J. Xu, K. Wang, S.Z. Zu, B.H. Han, Z. Wei, Hierarchical nanocomposites of polyaniline nanowire arrays on graphene oxide sheets with synergistic effect for energy storage, ACS Nano 4 (2010) 5019–5026.
[29] W.A. Marmisollé, O. Azzaroni, Recent developments in the layer-by-layer assembly of polyaniline and carbon nanomaterials for energy storage and sensing applications. From synthetic aspects to structural and functional characterization, Nanoscale 8 (2016) 9890–9918.
[30] K. Ariga, Y. Yamauchi, G. Rydzek, Q. Ji, Y. Yonamine, K.C.-W. Wu, et al., Layer-by-layer Nanoarchitectonics: Invention, Innovation, and Evolution, Chem. Lett. 43 (2014) 36–68.
[31] J.J. Richardson, M. Bjornmalm, F. Caruso, Technology-driven layer-by-layer assembly of nanofilms, Science 348 (2015) aaa2491-1-11.
[32] J. Yue, A. Epstein, XPS study of self-doped conducting polyaniline and parent systems, Macromolecules 24 (1991) 4441–4445.
[33] A.M. Kenwright, W.J. Feast, P. Adams, A.J. Milton, A.P. Monkman, B.J. Say, Solution-state carbon-13 nuclear magnetic resonance studies of polyaniline, Polymer 33 (1992) 4292–4298.
[34] C. Menardo, M. Nechtschein, A. Rousseau, J.P. Travers, P. Hany, Investigation on the structure of polyaniline: 13C n.m.r. and titration studies, Synth. Met. 25 (1988) 311–322.
[35] S. Kaplan, E.M. Conwell, A.F. Richter, A.G. MacDiarmid, Solid-state 13C NMR characterization of polyanilines, J. Am. Chem. Soc. 110 (1988) 7647–7651.
[36] G. Montaudo, F. Samperi, M.S. Montaudo, Characterization of synthetic polymers by MALDI-MS, Prog. Polym. Sci. 31 (2006) 277–357.
[37] R. Murgasova, D.M. Hercules, MALDI of synthetic polymers—An update, Int. J. Mass Spectrom. 226 (2003) 151–162.
[38] W. Armada, G. Contrafatti, L. Lizarraga, E.M. Andrade, F.V. Molina, Electrochemomechanical properties of aniline/2-methoxyaniline copolymers, J. Electroanal. Chem. 625 (2009) 75–81.
[39] I. Folch, S. Borrós, D.B. Amabilino, J. Veciana, Matrix-assisted laser desorption/ionization time-of-flight mass spectrometric analysis of some conducting polymers, J. Mass Spectrom. 35 (2000) 550–555.
[40] J. Laska, J. Widlarz, Spectroscopic and structural characterization of low molecular weight fractions of polyaniline, Polymer 46 (2005) 1485–1495.
[41] A.R. Dolan, T.D. Wood, Analysis of polyaniline oligomers by laser desorption ionization and solventless MALDI, J. Am. Soc. Mass Spectrom. 15 (2004) 893–899.
[42] A.R. Dolan, T.D. Wood, Synthesis and characterization of low molecular weight oligomers of soluble polyaniline by electrospray ionization mass spectrometry, Synth. Met. 143 (2004) 243–250.
[43] P.R. Sajanlal, T.S. Sreeprasad, A.S. Nair, T. Pradeep, Wires, plates, flowers, needles, and core-shells: Diverse nanostructures of gold using polyaniline templates, Langmuir 24 (2008) 4607–4614.
[44] M. Aono, Y. Bando, K. Ariga, Nanoarchitectonics: Pioneering a New Paradigm for Nanotechnology in Materials Development, Adv. Mater. 24 (2012) 150–151.
[45] K. Ariga, Q. Ji, W. Nakanishi, J.P. Hill, M. Aono, Nanoarchitectonics: a new materials horizon for nanotechnology, Mater. Horiz. 2 (2015) 406–413.
[46] M. Aono, K. Ariga, The Way to Nanoarchitectonics and the Way of Nanoarchitectonics, Adv. Mater. 28 (2016) 989–992.
[47] J.H. Cheung, W.B. Stockton, M.F. Rubner, Molecular-Level Processing of Conjugated Polymers. 3. Layer-by-Layer Manipulation of Polyaniline via Electrostatic Interactions, Macromolecules 30 (1997) 2712–2716.
[48] W.B. Stockton, M.F. Rubner, Molecular-Level Processing of Conjugated Polymers. 4. Layer-by-Layer Manipulation of Polyaniline via Hydrogen-Bonding Interactions, Macromolecules 30 (1997) 2717–2725.
[49] N.I. Kovtyukhova, T.E. Mallouk, Ultrathin anisotropic films assembled from individual single-walled carbon nanotubes and amine polymers, J. Phys. Chem. B 109 (2005) 2540–2545.
[50] A.K. Sarker, J.-D. Hong, Layer-by-Layer Self-Assembled Multilayer Films Composed of Graphene/Polyaniline Bilayers: High-Energy Electrode Materials for Supercapacitors, Langmuir 28 (2012) 12637–12646.
[51] A.K. Sarker, J.-D. Hong, Electrochemical reduction of ultrathin graphene oxide/polyaniline films for supercapacitor electrodes with a high specific capacitance, Colloids Surfaces A Physicochem, Eng. Asp. 436 (2013) 967–974.
[52] J.-W. Jeon, S.R. Kwon, J.L. Lutkenhaus, Polyaniline nanofiber/electrochemically reduced graphene oxide layer-by-layer electrodes for electrochemical energy storage, J. Mater. Chem. A 3 (2015) 3757–3767.
[53] G.S. Braga, L.G. Paterno, J.P.H. Lima, F.J. Fonseca, A.M. de Andrade, Influence of the deposition parameters on the morphology and electrical conductivity of PANI/PSS self-assembled films, Mater. Sci. Eng. C 28 (2008) 555–562.
[54] K. Sheng, H. Bai, Y. Sun, C. Li, G. Shi, Layer-by-layer assembly of graphene/polyaniline multilayer films and their application for electrochromic devices, Polymer 52 (2011) 5567–5572.
[55] T. Lee, T. Yun, B. Park, B. Sharma, H.-K. Song, B.-S. Kim, Hybrid multilayer thin film supercapacitor of graphene nanosheets with polyaniline: importance of establishing intimate electronic contact through nanoscale blending, J. Mater. Chem. 22 (2012) 21092–21099.

[56] N. Hyder, S.W. Lee, F.C. Cebeci, D.J. Schmidt, Y. Shao-Horn, P.T. Hammond, Layer-by-Layer Assembled Polyaniline Nano fi ber/Multiwall Carbon Nanotube Thin Film Electrodes for High-Power and High-Energy Storage Applications, ACS Nano 5 (2011) 8552–8561.
[57] J.W. Jeon, J. O'Neal, L. Shao, J.L. Lutkenhaus, Charge storage in polymer acid-doped polyaniline-based layer-by-layer electrodes, ACS Appl. Mater. Interfaces 5 (2013) 10127–10136.
[58] J. Ginder, A. Epstein, Role of ring torsion angle in polyaniline: Electronic structure and defect states, Phys. Rev. B 41 (1990) 10674–10685.
[59] J.G. Masters, J.M. Ginder, A.G. Macdiarmid, A.J. Epstein, Thermochromism in the insulating forms of polyanilne: role of ring-torsional conformation, J. Chem. Phys. 96 (1992) 4768–4778.
[60] J.E. Albuquerque, L.H.C. Mattoso, D.T. Balogh, R.M. Faria, J.G. Masters, A.G. MacDiarmid, A simple method to estimate the oxidation state of polyanilines, Synth. Met. 113 (2000) 19–22.
[61] R.P. McCall, J.M. Ginder, J.M. Leng, H.J. Ye, S.K. Manohar, J.G. Masters, et al., Spectroscopy and defect states in polyaniline, Phys. Rev. B 41 (1990) 5202–5213.
[62] D. Chinn, J. DuBow, J. Li, J. Janata, M. Josowicz, Comparison of Chemically and Electrochemically Prepared Polyaniline Films. 2. Optical Properties, Chem. Mater. 7 (1995) 1510–1518.
[63] D. Kumar, Electrochemical and optical behaviour of conducting polymer: poly (o-toluidine), Eur. Polym. J. 35 (1999) 1919–1923.
[64] C. Sanchís, H.J. Salavagione, J. Arias-Pardilla, E. Morallón, Tuning the electroactivity of conductive polymer at physiological pH, Electrochim. Acta 52 (2007) 2978–2986.
[65] W.A. Marmisollé, O. Azzaroni, Recent developments in the layer-by-layer assembly of polyaniline and carbon nanomaterials for energy storage and sensing applications. From synthetic aspects to structural and functional characterization, Nanoscale 8 (2016) 9890–9918.
[66] J. Tang, X. Jing, B. Wang, F. Wang, Infrared spectra of soluble polyaniline, Synth. Met. 24 (1988) 231–238.
[67] Y. Furukawa, F. Ueda, Y. Hyodo, I. Harada, T. Nakajima, T. Kawagoe, Vibrational spectra and structure of polyaniline, Macromolecules 21 (1988) 1297–1305.
[68] R.A. Weiss, A. Sen, C.L. Willis, L.A. Pottick, Block copolymer ionomers: 1. Synthesis and physical properties of sulphonated poly(styrene-ethylene/butylene-styrene), Polymer 32 (1991) 1867–1874.
[69] C.R. Martins, G. Ruggeri, M.A. De Paoli, Synthesis in Pilot Plant Scale and Physical Properties of Sulfonated Polystyrene, J. Braz. Chem. Soc. 14 (2003) 797–802.
[70] D. Krishnamurti, R. Somashekar, Mesomorphic Behaviour of Dodecyl Benzene Sulfonic Acid and Its Sodium Salt, Mol. Cryst. Liq. Cryst. 65 (1981) 3–22.
[71] B.L. Rivas, G.V. Seguel, Poly (acrylic acid-co-maleic acid)–metal complexes with copper(II), cobalt(II), and nickel(II) Synthesis characterization and structure of its metal chelates, Polyhedron 18 (1999) 2511–2518.
[72] M. Ibrahim, A. Nada, D.E. Kamal, Density functional theory and FTIR spectroscopic study of carboxyl group, Indian J. Pure Appl. Phys. 43 (2005) 911–917.
[73] S. Kumar, F. Gaillard, G. Bouyssoux, A. Sartre, High-resolution XPS studies of electrochemically synthesized conducting polyaniline films, Synth. Met. 36 (1990) 111–127.
[74] C. Hennig, K.H. Hallmeier, R. Szargan, XANES investigation of chemical states of nitrogen in polyaniline, Synth. Met. 92 (1998) 161–166.
[75] S. Golczak, a Kanciurzewska, M. Fahlman, K. Langer, J. Langer, Comparative XPS surface study of polyaniline thin films, Solid State Ionics. 179 (2008) 2234–2239.
[76] E. Kang, K. Neoh, K. Tan, X-ray photoelectron spectroscopic characterization of protonation of polyaniline films by polymeric acids, Polymer 35 (1994) 3193–3199.
[77] N. Graf, E. Yegen, T. Gross, A. Lippitz, W. Weigel, S. Krakert, et al., XPS and NEXAFS studies of aliphatic and aromatic amine species on functionalized surfaces, Surf. Sci. 603 (2009) 2849–2860.
[78] X. Song, Y. Ma, C. Wang, P.M. Dietrich, W.E.S. Unger, Y. Luo, Effects of Protonation Hydrogen Bonding, and Photodamaging on X-ray Spectroscopy of the Amine Terminal Group in Aminothiolate Monolayers, J. Phys. Chem. C. 116 (2012) 12649–12654.
[79] A.M. Bonastre, M. Sosna, P.N. Bartlett, An analysis of the kinetics of oxidation of ascorbate at poly(aniline)-poly(styrene sulfonate) modified microelectrodes, Phys. Chem. Chem. Phys. 13 (2011) 5365–5372.
[80] P.N. Bartlett, E.N.K. Wallace, The oxidation of ascorbate at poly(aniline)–poly (vinylsulfonate) composite coated electrodes, Phys. Chem. Chem. Phys. 3 (2001) 1491–1496.
[81] J. Cong, Y. Chen, J. Luo, X. Liu, Fabrication of graphene/polyaniline composite multilayer films by electrostatic layer-by-layer assembly, J.Solid State Chem. 218 (2014) 171–177.
[82] W.A. Marmisollé, M.I. Florit, D. Posadas, Acid-Base Equilibrium in Conducting Polymers. The case of Reduced Polyaniline, J. Electroanal. Chem. 734 (2014) 10–17.
[83] A.J. Bard, L.R. Faulkner, Electrochemical Methods. Fundamentals and Applications, 2nd ed., USA, 2001.
[84] A.M. Pisoschi, A. Pop, A.I. Serban, C. Fafaneata, Electrochemical methods for ascorbic acid determination, Electrochim. Acta. 121 (2014) 443–460.
[85] D. Zhou, J. Xu, H. Chen, H. Fung, Ascorbate Sensor Based on Self-Doped Polyaniline, Electroanalysis (1997) 1185–1188.
[86] R.A. Durst, A.J. Baumner, R.W. Murray, R.P. Buck, C.P. Andrieux, Chemically modified electrodes: Recommended terminology and definitions, Pure Appl. Chem. 69 (1997) 1317–1324.
[87] J. Luo, Y. Chen, Q. Ma, R. Liu, X. Liu, Layer-by-layer self-assembled hybrid multilayer films based on poly(sodium 4-styrenesulfonate) stabilized graphene with polyaniline and their electrochemical sensing properties, RSC Adv. 3 (2013) 17866–17873.
[88] J. Luo, R. Liu, X. Liu, Layer-by-layer assembled ionic-liquid functionalized graphene/polyaniline nanocomposite with enhanced electrochemical sensing properties, J. Mater. Chem. C 2 (2014) 4818–4827.
[89] F. Qu, M. Yang, J. Jiang, G. Shen, R. Yu, Amperometric biosensor for choline based on layer-by-layer assembled functionalized carbon nanotube and polyaniline multilayer film, Anal. Biochem. 344 (2005) 108–114.
[90] Z. Hu, J. Xu, Y. Tian, R. Peng, Y. Xian, Q. Ran, et al., Layer-by-layer assembly of poly (sodium 4-styrenesulfonate) wrapped multiwalled carbon nanotubes with polyaniline nanofibers and its electrochemistry, Carbon N. Y. 48 (2010) 3729–3736.
[91] E. Maza, J.S. Tuninetti, N. Politakos, W. Knoll, S. Moya, O. Azzaroni, pH-responsive ion transport in polyelectrolyte multilayers of poly (diallyldimethylammonium chloride) (PDADMAC) and poly(4-styrenesulfonic acid-co-maleic acid) (PSS-MA) bearing strong- and weak anionic groups, Phys. Chem. Chem. Phys. 17 (2015) 29935–29948.